---

**Article:**
Liu, T.Y., Zhu, Z.Q. orcid.org/0000-0001-7175-3307, Shuang, B. et al. (3 more authors) (2021) An online position error correction method for sensorless control of permanent magnet synchronous machine with parameter mismatch. IEEE Access, 9. pp. 135708-135722.

https://doi.org/10.1109/access.2021.3116515

---

IEEE Access
Multidisciplinary | Rapid Review | Open Access Journal

Received August 25, 2021, accepted September 20, 2021, date of publication September 29, 2021, date of current version October 11, 2021.

*Digital Object Identifier 10.1109/ACCESS.2021.3116515*

# An Online Position Error Correction Method for Sensorless Control of Permanent Magnet Synchronous Machine With Parameter Mismatch

**T. Y. LIU[1], Z. Q. ZHU[1], (Fellow, IEEE), B. SHUANG[1], Z. Y. WU[2], DAVID A. STONE[1], AND MARTIN P. FOSTER[1]**

[1]Department of Electronic and Electrical Engineering, The University of Sheffield, Sheffield S1 3JD, U.K.
[2]Sheffield-Siemens Gamesa Renewable Energy (S[2]GRE) Research Centre, Sheffield S3 7HQ, U.K.

Corresponding author: Z. Q. Zhu (z.q.zhu@sheffield.ac.uk)

This work was supported by the U.K. Engineering and Physical Sciences Research Council (EPSRC) Prosperity Partnership "A New Partnership in Offshore Wind" under Grant EP/R004900/1.

**ABSTRACT** To eliminate the influence of parameter mismatch for fundamental model based sensorless methods, an effective online position error correction method is proposed for permanent magnet synchronous machines in this paper. Based on the derived position error mechanism, i.e. the error varies proportionally to the *dq*-axis currents, the proposed method injects a sinusoidal current signal with a small amplitude and low frequency into the *d*- or *q*-axis current for a short period. During injection, the corresponding sinusoidal response for current injection can be acquired from the estimated speed of the sensorless position observer. It is found that the amplitude of the response in the estimated speed decreases as the parameter mismatch reduces, and eventually reaches a minimum if there is no parameter mismatch. Thus, by applying the least mean square (LMS) algorithm, the amplitude of the response in the estimated speed can be minimised as the parameters are adaptively adjusted to the actual values, and then the position error can be corrected. The proposed method is validated through experiments on a permanent magnet generator drive system.

**INDEX TERMS** Extended electromotive force (E-EMF), least mean square (LMS), permanent magnet synchronous machine (PMSM), sensorless.

## I. INTRODUCTION

Permanent magnet (PM) synchronous machines (PMSMs) are continuously attracting more attention in recent years due to their superior performance and noticeable advantages, such as high efficiency, large torque and power density, and fast speed response. In order to achieve a reliable and high-performance field-oriented control (FOC) in real applications, accurate rotor position information is necessary. Generally, mechanical sensors, such as encoder or resolver, are used to acquire accurate rotor position information. However, the use of these sensors will increase the cost and complexity, and reduce the reliability of a whole drive system. Therefore, the rotor position sensorless techniques are preferred.

Over the last three decades, many sensorless methods have been proposed [1]–[20], [32]–[35]. Among these methods, the most developed are saliency tracking based methods [1]–[3], [33]–[35], and fundamental model-based methods [4]–[20], [32]. The former type of methods detects rotor position information by injecting various high-frequency (HF) signals to produce corresponding responses. These methods usually depend on the presence of the anisotropic property of the machine and are particularly applied for low-speed range or even standstill. Once above a certain speed, as the back electromotive force (EMF) is detectable, the fundamental model-based methods are favored. These methods use electrical signals to estimate back-EMF [4]–[11] or flux-linkage [12]–[14], which contains the information of the rotor position. Since these methods are based on the mathematical model of the machines, they generally have a strong dependency on the accuracy of the machine parameters. In a real application, the machine parameters vary at different operating conditions, temperatures, and magnetic saturation effects. If the nominal parameters used in these methods are different from the actual machine parameters

The associate editor coordinating the review of this manuscript and approving it for publication was Feifei Bu.

(i.e. parameter mismatch), a DC offset error appears in the estimated position [9]–[12], [15]–[20].

In order to reduce the effects caused by parameter mismatch, many methods have been proposed, and they can be generally classified into two categories: offline approaches [9], [12], [15], [22] and online algorithms [3], [16]–[20]. One typical offline solution is to fit curves or to build lookup tables of the parameters based on finite element analysis (FEA) results [15]. Others, such as in [9], the q-axis inductance is measured with the help of an encoder. In [12], a pre-determined artificial inductance is introduced to reduce the rotor position error. Although these methods are simple and straightforward, the results from offline measurements or approaches are not always representative in practical applications, and the offline tests are usually cumbersome. Therefore, some online algorithms, such as model reference adaptive system (MRAS) [16]–[18] algorithms, recursive least square (RLS) algorithm [20], [27], affine projection algorithm (APA) [28] and extended Kalman filter (EKF) [25], have been applied to reduce the influence of parameter mismatch in the sensorless application. MRAS algorithm is applied in [16]–[18] to eliminate the influence of resistance mismatch at low-speed whilst the inductances are set to their nominal values. However, it has been shown that the resistance mismatch along with the inverter irregularities have a limited effect on rotor position estimation in medium- to the high-speed ranges, where the error is dominated by q-axis inductance mismatch [8]–[12]. In [20], the system identification methodology is applied to determine the parameters online with the help of the RLS algorithm. However, this method, along with other previously mentioned online algorithms, tries to solve the machine parameters through mathematical model of the PMSMs, and thus, have ill-convergence and rank deficient problems [21]. To overcome the above issues, [27] proposes a method to estimate online the parameters based on two timescale RLS algorithms. The fast RLS algorithm segment estimates the inductances and the slow one identifies the stator resistance, respectively. A similar method is also adopted in [28] where two APAs are used. A possible drawback of this type of method is that the inaccuracy in the estimation of inductance reflects the imprecision of resistance calculation. In other methods, such as in [3], all parameters are determined at a standstill situation with the accurate position determined by a high-frequency injection method, which cannot be adaptively changed for various operating conditions.

As aforementioned, the parameter mismatch, which leads to DC offset error in the position estimation, is a common issue for fundamental model-based methods [11]. In this paper, the authors look at the problem from a different view. Instead of focusing on the mathematical model for parameter estimation, the position error mechanism is derived, and it shows that: (a) only the mismatch of $R_s$ and $L_q$ (not $L_d$) could cause position error; (b) the position error has the same trend as the current variation under the situation of the parameter deviation; (c) the position error due to multiple parameter deviations can be separated or decoupled. Therefore, by using this core mechanism, an online position error correction method is proposed to minimise the influence of parameter mismatch. In the proposed method, the effects of parameter mismatch are exposed by extra sinusoidal current signal stimulation, and the signal has a relatively small amplitude and a low frequency. To be more specific, the sinusoidal current signal can be injected into the $d$- or $q$-axis of the current for a short period to acquire the corresponding estimated speed responses from the sensorless position observer. If the parameters are incorrectly applied, there would be a resultant AC component that has the same frequency as the injection current signal appearing in the estimated speed and position, and the amplitude of this AC component decreases as the degree of parameter mismatch reduces. Since the amplitude eventually reaches a minimum when the mismatch disappears, with the help of the least mean square (LMS) algorithm [21], [26], the parameter can be considered as the weight factor that is adaptively trained until the amplitude of the AC component reaches a minimum value. Then, the accurate parameters can be determined, and the rotor position error can be corrected. The proposed method does not try to solve the machine parameters through the mathematical model of PMSMs as the conventional methods, but could adaptively correct the rotor position error due to parameter mismatch based on the position error mechanism that is derived. Moreover, the effects of $L_q$ and $R_s$ deviations on the position estimation can be decoupled in the proposed method, which means that each parameter correction can be independently achieved without considering the inaccuracy of other parameters. Thus, the issues of ill-convergence and rank deficiency can be prevented.

In this paper, the extended-EMF (E-EMF) based observer in the estimated synchronous rotating reference frame [7] is used to investigate the influence of parameter mismatch and sensorless control. Since the proposed method is based on a fundamental model-based sensorless observer, and the sinusoidal current signal with a relatively low frequency and a small amplitude is only injected for a short duration of time (a few seconds) to minimise the influence of parameter mismatch, it can be distinguished from the HF signal injection sensorless methods and the indirect flux detection by online reactance measurement (INFORM) method [35]. The HF signal injection methods, which are saliency tracking based, require injected signal to be applied continuously. The INFORM method, on the other hand, is a transient injection based technique, which injects HF impulse voltage vectors to obtain current transient responses based on machine saliency. Moreover, by considering the potential effects from the extra current signal injection, the proposed method can be employed when the parameters need to be corrected only at a specific load point, and a measure has been taken so that the whole correction procedure can be achieved in a short period of time. Additionally, as the parameters may be corrected only once, the method can also be employed during the drive commissioning to build lookup tables. Through these

measures, its impact on the drive system efficiency, voltage usage and torque ripple can be kept minimum.

The rest of this paper is organized as follows. In Section II, the E-EMF sensorless method in dq reference frame is presented. The effect of parameter mismatch on position estimation is investigated and discussed in Section III. The position correction method is proposed and discussed in details in Section IV. The proposed method is verified by the experimental results on a PMSM drive system in section V. Finally, a conclusion is given in Section VI.

## II. CONVENTIONAL EXTENDED-EMF SENSORLESS METHOD

### A. MATHEMATICAL MODEL

By considering the apparent inductance, incremental inductance and cross-coupling inductance, the extended-EMF (E-EMF) model in the synchronous rotating reference frame (RRF) can be expressed as (1) [4], [5]. From mathematical manipulation of the conventional model, the impedance matrix of the $dq$-axis voltage equations becomes symmetrical by applying the E-EMF concept [6], [7]. Then, the model can be used for the development of sensorless control. This model is more general and complete and is suitable for both interior (I-) PMSM and surface mounted (S-) PMSM.

$$\begin{bmatrix} v_d \\ v_q \end{bmatrix} = \begin{bmatrix} R_s + L_d^{inc}p - \omega_r L_{qd}^a & -\omega_r L_q^a + L_{dq}^{inc}p \\ \omega_r L_q^a - L_{dq}^{inc}p & R_s + L_d^{inc}p - \omega_r L_{qd}^a \end{bmatrix} \times \begin{bmatrix} i_d \\ i_q \end{bmatrix} + \begin{bmatrix} 0 \\ E_{ex}^{imp} \end{bmatrix} \quad (1)$$

where

$$E_{ex} = \omega_r \psi_f + \left(\omega_r L_d^a - \omega_r L_q^a + L_{qd}^{inc}p + L_{dq}^{inc}p\right) i_d + \left(L_q^{inc}p - L_d^{inc}p + \omega_r L_{dq}^a + \omega_r L_{qd}^a\right) i_q \quad (2)$$

$E_{ex}$ is called E-EMF; $p$ is a derivative operator; $v_d$, $v_q$ and $i_d$, $i_q$ represent the voltages and currents in $dq$-axes, respectively; $R_s$ is the stator resistance; $L_d$, $L_q$ are the $d$- and $q$-axis inductances, $L_{dq}$ and $L_{qd}$ are mutual inductances, and $\psi_f$ is the PM flux-linkage; $\omega_r$ is the rotor electrical angular velocity. The inductances with the superscript of "inc" or "a" represent the incremental and apparent inductances, respectively.

(1) can be transformed into the estimated RRF as:

$$\begin{bmatrix} v_d^e \\ v_q^e \end{bmatrix} = \begin{bmatrix} R_s + L_d^{inc}p - \omega_r^e L_{qd}^a & -\omega_r^e L_q^a + L_{dq}^{inc}p \\ \omega_r^e L_q^a - L_{dq}^{inc}p & R_s + L_d^{inc}p - \omega_r^e L_{qd}^a \end{bmatrix} \times \begin{bmatrix} i_d^e \\ i_q^e \end{bmatrix} + \begin{bmatrix} e_d^e \\ e_q^e \end{bmatrix} \quad (3)$$

where

$$\begin{bmatrix} e_d^e \\ e_q^e \end{bmatrix} = E_{ex} \begin{bmatrix} \sin(\Delta\theta) \\ \cos(\Delta\theta) \end{bmatrix} + \left(\omega_r^e - \omega_r\right) \begin{bmatrix} L_q^a i_q^e + L_{qd}^a i_d^e \\ -L_q^a i_d^e + L_{qd}^a i_q^e \end{bmatrix} \quad (4)$$

The superscript "$e$" represents the estimated RRF that lags by $\Delta\theta$ from the actual RRF. After the convergence of the closed-loop position observer, $\Delta\theta$ will be driven to zero, and the difference between the estimated and actual speed will disappear. Thus, the second term in the right hand of (4) can be neglected.

### B. POSITION ESTIMATION

The rotor position can be estimated by observing the position of the E-EMF in the estimated RRF. To achieve this, the concept of the reduced-order observer in [7] can be used, which is constructed as:

$$\begin{cases} \dot{\hat{\boldsymbol{i}}} = \tilde{\boldsymbol{A}}_{1,1}\boldsymbol{i} + \tilde{\boldsymbol{A}}_{1,2}\hat{\boldsymbol{e}} + \tilde{\boldsymbol{B}}_1\mathbf{v} \\ \dot{\hat{\boldsymbol{e}}} = \mathbf{G}(\dot{\hat{\boldsymbol{i}}} - \dot{\boldsymbol{i}}) \end{cases} \quad (5)$$

where

$$\begin{aligned} \boldsymbol{i} &= \begin{bmatrix} i_d^e & i_q^e \end{bmatrix}^T, \quad \mathbf{e} = \begin{bmatrix} e_d^e & e_q^e \end{bmatrix}^T, \\ \mathbf{v} &= \begin{bmatrix} V_d & V_q \end{bmatrix}^T \\ &= \begin{bmatrix} v_d^e + \omega_r^e \tilde{L}_q i_q^e - \tilde{L}_{dq} p i_q^e & v_q^e - \omega_r^e \tilde{L}_q i_d^e + \tilde{L}_{dq} p i_d^e \end{bmatrix}^T, \\ \tilde{\boldsymbol{A}}_{1,1} &= -\frac{\tilde{R}_s - \omega_r^e \tilde{L}_{qd}}{\tilde{L}_d}\mathbf{I}, \quad \tilde{\boldsymbol{A}}_{1,2} = -\frac{1}{\tilde{L}_d}\mathbf{I}, \\ \tilde{\boldsymbol{B}}_{1,1} &= \frac{1}{\tilde{L}_d}\mathbf{I}, \quad \mathbf{I} = \begin{bmatrix} 1 & 0 \\ 0 & 1 \end{bmatrix} \end{aligned} \quad (6)$$

In (5), $\boldsymbol{i}$ and E-EMF "$\boldsymbol{e}$" are considered as the state variables. The input of the system is the voltage $\boldsymbol{v}$ of the stator, and it is formed in order to eliminate the cross-coupling terms [7], while the output of the system is the stator current $\boldsymbol{i}$, and $\boldsymbol{G}$ is the observer feedback gain. The symbols with "^" are the estimated state variables, the tilde ($\sim$) represents the nominal value of the parameter. If the observer poles are well designed, the estimation error of the observer converges to zero and has a good dynamic performance. By applying the reduced-order observer, the estimated E-EMF can be acquired as:

$$\begin{bmatrix} \hat{e}_d^e \\ \hat{e}_q^e \end{bmatrix} = E_{ex} \begin{bmatrix} -\sin\left(\Delta\hat{\theta}\right) \\ \cos\left(\Delta\hat{\theta}\right) \end{bmatrix} \quad (7)$$

Then, the estimated position error $\Delta\hat{\theta}$ can be calculated by:

$$\Delta\hat{\theta} = \tan^{-1}\left(-\hat{e}_d^e \Big/ \hat{e}_q^e\right) \quad (8)$$

A PI controller is generally used to force $\Delta\hat{\theta}$ to zero. When the phase voltages and currents can be precisely obtained and the machine parameters are accurately given to the observer, the exact rotor position can be estimated.

## III. EFFECT OF PARAMETER MISMATCH ON POSITION ESTIMATION

In real applications, it is challenging to obtain accurate parameter values of an electrical machine, since the actual parameters vary with temperature, saturation effect, and load condition, etc. For conventional model based sensorless

methods, only one set of nominal parameter values are used in the EMF or flux-linkage estimator. Therefore, when actual parameters vary, the parameter mismatch issue is introduced, which may not only cause estimated position error but also deteriorate the performance of the position observer and control system.

In this section, the influence of the parameter mismatch on rotor position estimation will be firstly investigated. The effect of mutual inductance is depended on the machine design and can be compensated by using the technique in [4]. In this paper, it is neglected and the rest three machine parameters are considered. To be more specific, they are phase resistance, $d$-axis inductance and $q$-axis inductance. Nevertheless, the effect of mutual inductance on the accuracy of the proposed method will be investigated in Section IV part E. Therefore, the relationship between the nominal $(\tilde{R}_s, \tilde{L}_d, \tilde{L}_q)$ and actual $(R_s, L_d, L_q)$ values of the parameters are defined as:

$$R_s = \tilde{R}_s + \Delta R_s \tag{9}$$

$$L_d = \tilde{L}_d + \Delta L_d \tag{10}$$

$$L_q = \tilde{L}_q + \Delta L_q \tag{11}$$

where the nominal parameters are those used in the position observer, and the parameters with "$\Delta$" represent the mismatched parameters. It should be mentioned that the PM flux linkage $\psi_f$ does not need to be considered here since it is not required when an E-EMF based observer is applied.

### A. RESISTANCE MISMATCH

When there is a phase resistance mismatch as (9), the difference between the estimated and actual derivative current state variables can be derived from (5) as:

$$\dot{\hat{\boldsymbol{i}}} - \dot{\boldsymbol{i}} = \left(\tilde{\boldsymbol{A}}_{1.1} - \boldsymbol{A}_{1.1}\right)\boldsymbol{i} + \boldsymbol{A}_{1,2}\left(\hat{\boldsymbol{e}} - \boldsymbol{e}\right) \tag{12}$$

If the feedback gain of the observer is well designed, then the estimation error of $\dot{\hat{\boldsymbol{i}}} - \dot{\boldsymbol{i}}$ can be assumed to converge to zero at steady-state, and the E-EMF estimation error can be acquired, which can be expressed as:

$$\boldsymbol{\varepsilon}_{\Delta R_s} = \hat{\boldsymbol{e}} - \boldsymbol{e} = \Delta R_s \boldsymbol{I}\boldsymbol{i} \tag{13}$$

where $\boldsymbol{\varepsilon}_{\Delta R_s} = \left[\varepsilon_{d,\Delta R_s}\ \varepsilon_{q,\Delta R_s}\right]^T$ are the errors of estimated E-EMF, and the subscript denotes the type of mismatched parameter.

### B. INDUCTANCE MISMATCH

In the case of mismatch in the $d$- or $q$-axis inductance, the difference between the estimated and actual derivative current state variables, $\dot{\hat{\boldsymbol{i}}} - \dot{\boldsymbol{i}}$, can be similarly derived, and then the error of the estimated E-EMF can be derived as:

$$\begin{cases} \boldsymbol{\varepsilon}_{\Delta L_d} = 0 \\ \boldsymbol{\varepsilon}_{\Delta L_q} = \Delta L_q \hat{\omega}_r \mathbf{J}\boldsymbol{i} \end{cases} \tag{14}$$

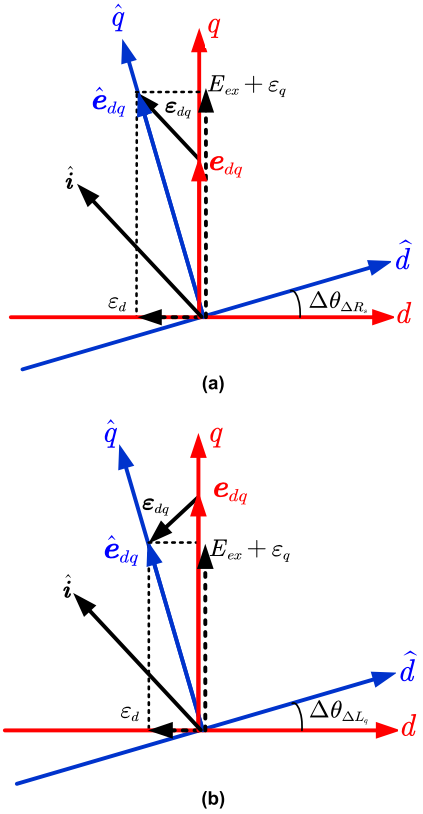


**FIGURE 1.** Space vector diagrams. (a) resistance mismatch. (b) q-axis inductance mismatch.

where $\boldsymbol{\varepsilon}_{\Delta L_d} = \left[\varepsilon_{d,\Delta L_d}\ \varepsilon_{q,\Delta L_d}\right]^T$, $\boldsymbol{\varepsilon}_{\Delta L_q} = \left[\varepsilon_{d,\Delta L_q}\ \varepsilon_{q,\Delta L_q}\right]^T$, and $\mathbf{J} = \begin{bmatrix} 0 & -1 \\ 1 & 0 \end{bmatrix}$. From (13) and (14), it can be observed that the E-EMF observer is less sensitive to the d-axis inductance mismatch. However, the stator resistance and q-axis inductance may cause the estimated error in the estimated E-EMF, and thus affect the position estimation accuracy [9]–[12].

### C. ESTIMATED POSITION ERROR DUE TO PARAMETER MISMATCH

From above, the E-EMF error $\boldsymbol{\varepsilon}$ can be considered as a vector that deviates the estimated E-EMF vector $\hat{\boldsymbol{e}}_{\boldsymbol{dq}}$ from the actual E-EMF vector $\boldsymbol{e}_{\boldsymbol{dq}}$, as shown in Fig. 1.

Then, the position error can be easily calculated by:

$$\Delta\theta_{par} = \tan^{-1}\left(\frac{\varepsilon_d}{E_{ex} + \varepsilon_q}\right) \tag{15}$$

where $\Delta\theta_{par}$ is the position error that is caused by the parameter mismatch and can be defined as $\Delta\theta_{par} = \theta_r - \hat{\theta}_r^e$.

By substituting (13) and (14) into (15) respectively, the influence of the parameter mismatch of phase resistance and inductance on the estimated position error can be derived as:

$$\Delta\theta_{\Delta R_s} = \tan^{-1}\left(\frac{\Delta R_s \hat{i}_d^e}{E_{ex} + \Delta R_s \hat{i}_q^e}\right) \tag{16}$$

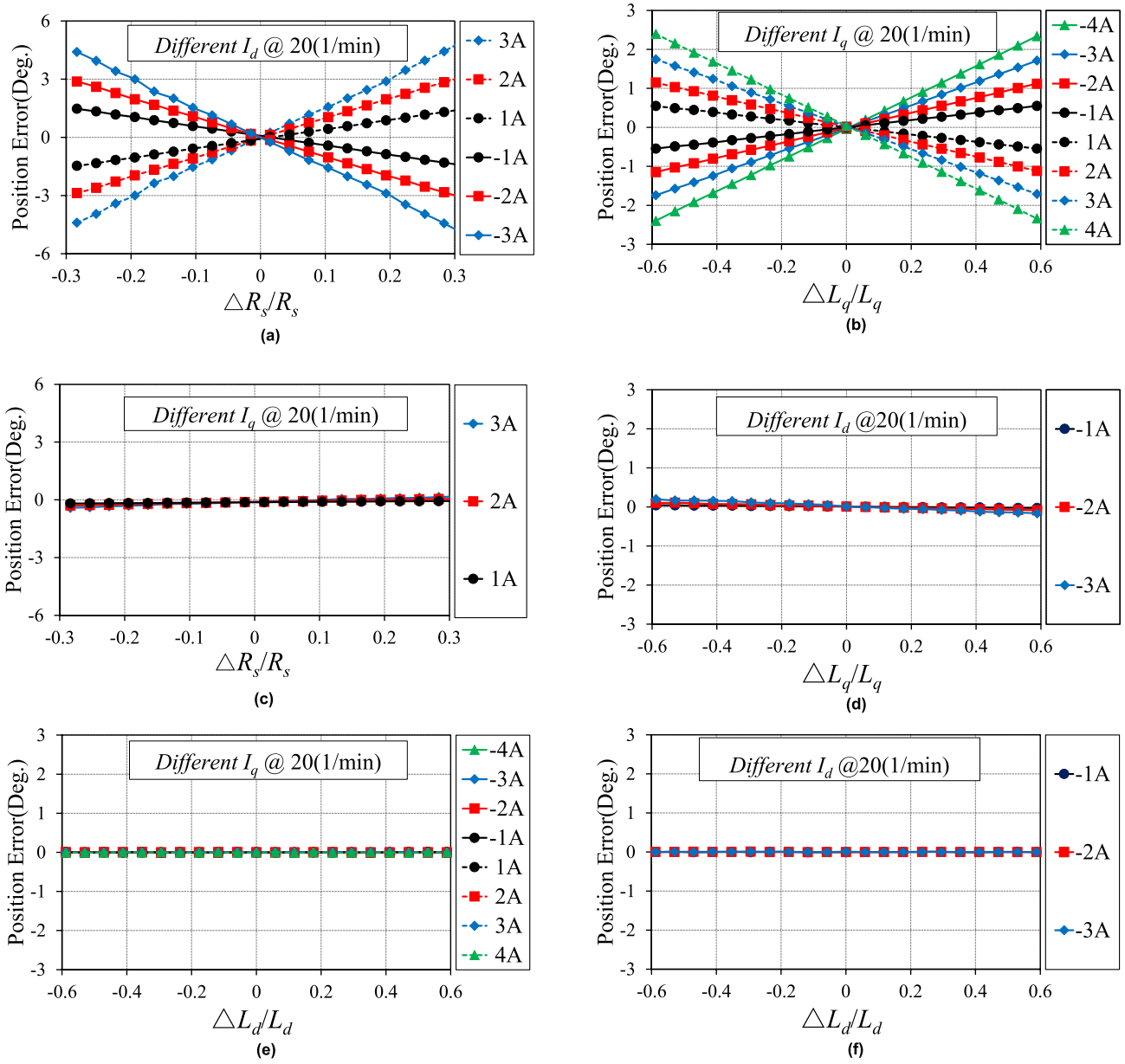


**FIGURE 2.** Measured position errors of E-EMF observer under different parameter mismatches and current levels at 20(1/min). (a) $\Delta R_s/R_s$ for different $I_d$. (b) $\Delta L_q/L_q$ for different $I_q$. (c) $\Delta R_s/R_s$ for different $I_q$. (d) $\Delta L_q/L_q$ for different $I_d$. (e) $\Delta L_d/L_d$ for different Iq. (f) $\Delta L_d/L_d$ for different $I_d$.

$$\begin{cases} \Delta\theta_{\Delta L_d} = 0 \\ \Delta\theta_{\Delta L_q} = \tan^{-1}\left(\dfrac{-\Delta L_q \hat{i}_q^e}{E_{ex}/\hat{\omega}_r^e + \Delta L_q \hat{i}_d^e}\right) \end{cases} \tag{17}$$

where $\Delta\theta_{\Delta R_s}$, $\Delta\theta_{\Delta L_d}$ and $\Delta\theta_{\Delta L_q}$ represent the estimated position errors caused by the mismatch in phase resistance and $d$- and $q$-axis inductances, respectively.

The above mathematical analysis has been verified experimentally on the vector-controlled drive system with the help of a high-resolution encoder. The details of the platform hardware are given in section V, and machine parameters are given in Table 1. Fig. 2 shows the experimental results at 20(1/min) of the rotor position error due to $\Delta R_s$, $\Delta L_q$ and $\Delta L_d$ when one axis current is varied and the other axis current is controlled to zero. To be more specific, in Fig. 2(a), at a given $I_d$ value, the error is proportional to $\Delta R_s$, whilst in Fig. 2(b), at a given $I_q$ value, the error is proportional to $\Delta L_q$. From another perspective, at a given $R_s$ (or $L_q$), the error is proportional to the $d$- (or $q$-) axis current level. However, if there is no mismatch in the parameters, the change in current should barely make any difference in terms of position error. In addition, from Fig. 2(c), it is observed that $\Delta R_s$ has barely introduced any position errors for different $I_q$ values, whilst in Fig. 2(d), when $L_q$ is mismatched, different $I_d$ level has little effect on position estimation accuracy. Moreover, from Figs. 2(e) and (f), it is found that $\Delta L_d$ has no effect on position estimation. Along with (16) and (17), these features can be concluded as a position error mechanism. That is, the position error is mainly caused by the parameter mismatch of $R_s$ and $L_q$, and the

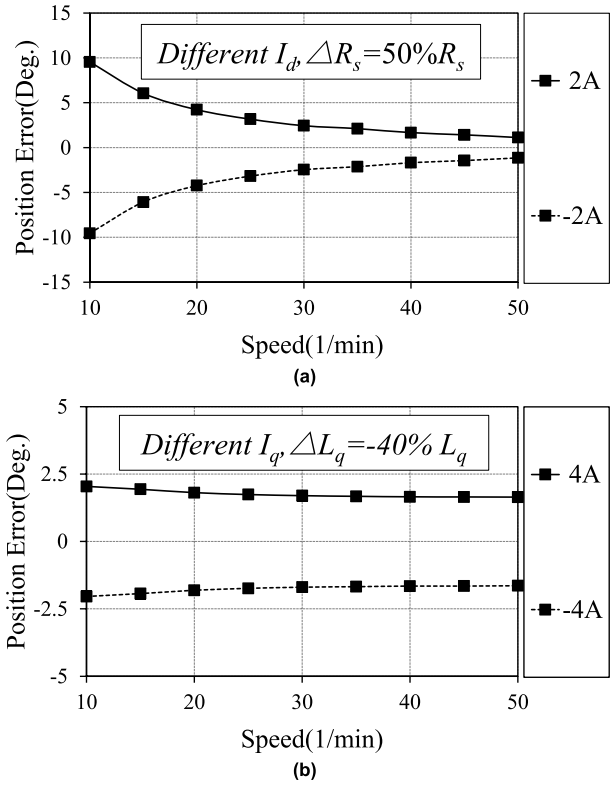


**FIGURE 3.** Measured position errors of E-EMF observer under different speed levels. (a) $R_s$ mismatch. (b) $L_q$ mismatch.

level of position error is proportionally varied according to $I_d$ for $\Delta R_s$ and $I_q$ for $\Delta L_q$. Furthermore, the effect of $\Delta R_s$ is hardly coupled with $I_q$ level, and nor $\Delta L_q$ with $I_d$ level. On the other hand, from (16) and Fig. 3(a), the position error due to $\Delta R_s$ decreases as the speed increases, while from (17) and Fig. 3(b), the error due to $\Delta L_q$ is independent of speed variation. Again, if there was no parameter mismatch, the position error would be zero and the speed becomes irrelevant.

On the other hand, the dynamic performance of the position estimation has been tested by the application of current impulse in the $dq$-axis currents. Figs. 4 (a), (b) and (c) are the experimental results of position error with $q$-axis current impulse (no load to half load) when the mismatches in parameters of $L_d$, $L_q$ and $R_s$ are considered, respectively. It can be clearly seen that the observer is less sensitive to $L_d$ and $R_s$ mismatch but more sensitive to $L_q$ mismatch under the $I_q$ impulse condition. Moreover, in Fig. 4(c), it should also be noticed that the more accurate the $L_q$ is, the less influence it has on the dynamic response of the observer. In Fig. 4(d), the dynamic performance is tested under the $d$-axis impulse condition for different $R_s$ mismatch levels. Again, the results show the $R_s$ mismatch effect on the dynamic performance of the position observer can be minimised when accurate $R_s$ is applied. Therefore, the parameter accuracy in the observer is important for the position estimation not only at steady state but also during the transient.

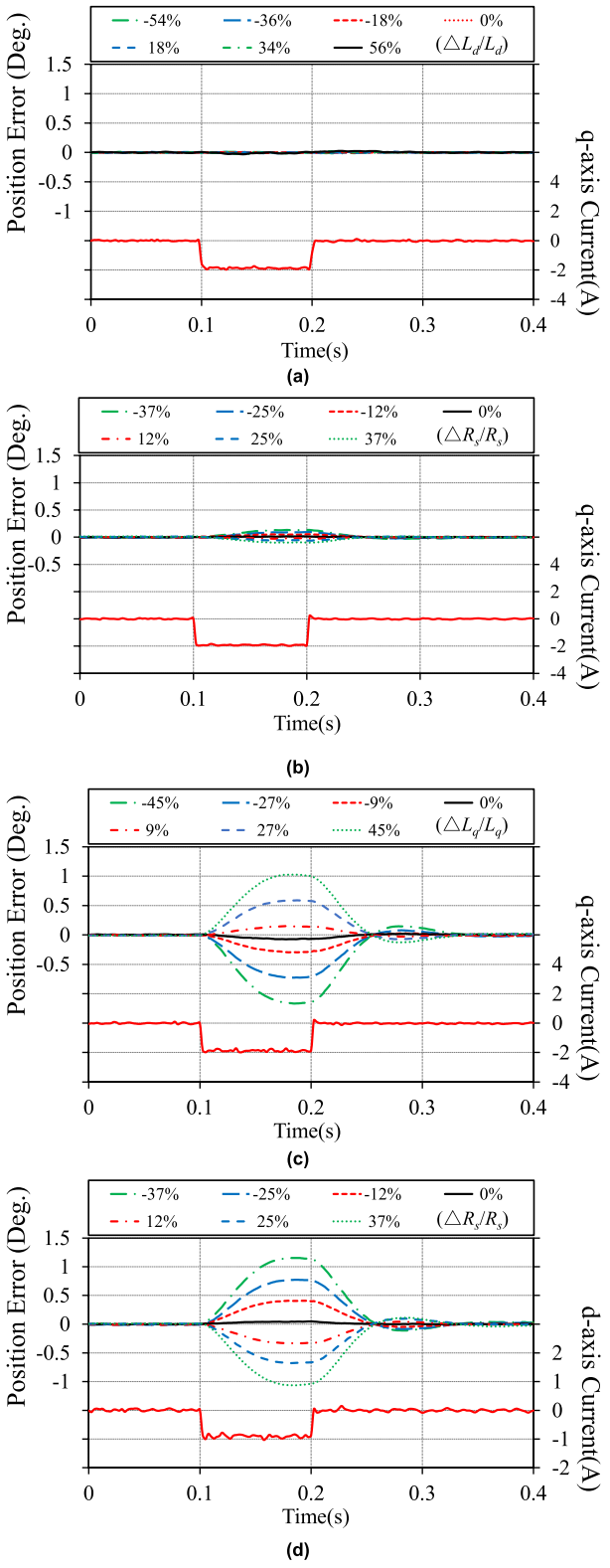


**FIGURE 4.** Measured position error dynamic response of E-EMF observer under q-axis current impulse tests. (a) $L_d$ mismatch (b) $R_s$ mismatch (c) $L_q$ mismatch; and d-axis current impulse test for (d) Rs mismatch.

## IV. PROPOSED POSITION CORRECTION TECHNIQUE

Since phase resistance and $q$-axis inductance mismatch can cause position error in the estimation, the error due to

**TABLE 1. Nominal values of machine parameters.**

| Parameters | Value | Parameters | Value |
|---|---|---|---|
| Inertia (kgm$^2$) | 1.51 | Phase resistance(Ω) | 3.9 |
| Rated current (A,peak) | 4 | Equ. phase resistance(Ω) | 4.1 |
| Rated torque (Nm) | 104 | Pole pairs | 16 |
| Rated speed(1/min) | 170 | d-inductances (mH) | 19.21 |
| Magnetic flux (Wb) | 1.03 | q-inductances (mH) | 19.21 |

parameter deviation may be generally written as (18) by combining (16) and (17):

$$\Delta\theta_{par} = \Delta\theta_{\Delta L_q} + \Delta\theta_{\Delta R_s} \approx K_{\Delta L_q}\hat{i}_q^e + K_{\Delta R_s}\hat{i}_d^e \quad (18)$$

where $K_{\Delta R_s}$ and $K_{\Delta L_q}$ are the mismatch factors and defined as:

$$K_{\Delta R_s} = \frac{\Delta R_s}{E_{ex} + \Delta R_s\hat{i}_q^e}, \quad K_{\Delta L_q} = -\frac{\Delta L_q}{E_{ex}/\hat{\omega}_r^e + \Delta L_q\hat{i}_d^e} \quad (19)$$

The error in (18) is composed of two parts, one related to $\Delta R_s$, and the other $\Delta L_q$. If each part of the mismatched parameter can be corrected independently, the whole position error can be eliminated, regardless of the level of currents. In the existing methods, the accurate parameters are normally achieved through the algorithms of parameter identification. All the parameters need to be identified based on the mathematical model of PMSMs, which cause the issue of ill-convergence and rank deficiency [21]. However, if the position error mechanism is considered, only two parameters are related to the position error, and they can be independently corrected through the proposed method. As aforementioned, if there is no parameter mismatch, the error will not respond to the current variation. Otherwise, at the presence of a parameter mismatch, the error would take the same trend as the current variation. Therefore, if the current can be purposely varied, e.g. by superimposing a sinusoidal current signal (20) with low frequency $\omega_{ac}$ and small amplitude $A_{ac}$ onto $d$- or $q$-axis current reference, the position error should vary at the same frequency of the sinusoidal current signal, unless there is no parameter mismatch.

$$i_{ac}^* = A_{ac}\sin\omega_{ac}t \quad (20)$$

It should be mentioned that, the frequency of injection should be low enough to make sure the estimated current track the current reference variation properly in the $dq$ reference frame, more details about how to choose the injection frequency and amplitude are shown in Section V, part B.

### A. AC SIGNAL SUPERIMPOSED ONTO Q-AXIS TO MINIMISE EFFECT OF Q-AXIS INDUCTANCE MISMATCH

The sinusoidal current signal can be superimposed onto $q$-axis current command $i_q^*$ for $L_q$ correction, and the estimated $q$-axis current can be expressed as:

$$\hat{i}_q^e = \hat{i}_{q,dc}^e + \hat{i}_{q,ac}^e \quad (21)$$

where the subscript "dc" or "ac" denotes the DC or AC components, respectively, $\hat{i}_{q,ac}^e$ is defined as the corresponding $q$-axis AC current component, and due to the current control, its frequency will keep the same as that of the injected sinusoidal current signal. Therefore, (18) can be rewritten as (22) when the extra signal is injected.

$$\begin{aligned}\Delta\theta_{\Delta L_q,ac} &\approx K_{\Delta L_q}\left(\hat{i}_{q,dc}^e + \hat{i}_{q,ac}^e\right) + \frac{\Delta R_s}{E_{ex} + \Delta R_s\left(\hat{i}_{q,dc}^e + \hat{i}_{q,ac}^e\right)}\hat{i}_{d,dc}^e \\ &= K_{\Delta L_q}\hat{i}_{q,dc}^e + K_{\Delta L_q}\hat{i}_{q,ac}^e + K_{\Delta R_s}\hat{i}_{d,dc}^e + K_{\Delta R_s,ac}\hat{i}_{d,dc}^e \\ &= \Delta\theta_{par} + K_{\Delta L_q}\hat{i}_{q,ac}^e + K_{\Delta R_s,ac}\hat{i}_{d,dc}^e \end{aligned} \quad (22)$$

where

$$K_{\Delta R_s,ac} = \frac{\Delta R_s^2\hat{i}_{q,ac}^e}{\left(E_{ex} + \Delta R_s\hat{i}_{q,dc}^e + \Delta R_s\hat{i}_{q,ac}^e\right)\left(E_{ex} + \Delta R_s\hat{i}_{q,dc}^e\right)} \quad (23)$$

In (22), two extra AC components $K_{\Delta L_q}\hat{i}_{q,ac}^e$ and $K_{\Delta R_s,ac}\hat{i}_{d,dc}^e$ appear in the position error due to sinusoidal current signal injection, and the amplitude $\left|K_{\Delta L_q}\hat{i}_{q,ac}^e\right| = K_{\Delta L_q}A'_{q,ac}$ ($A'_{q,ac} = \left|\hat{i}_{q,ac}^e\right|$) has a close relationship with $L_q$ mismatch ($\Delta L_q$) while $\left|K_{\Delta R_s,ac}\hat{i}_{d,dc}^e\right|$ is independent of $\Delta L_q$. To be more specific, if the degree of $\Delta L_q$ decreases ($K_{\Delta L_q}$ decreases), the amplitude of the AC component $K_{\Delta L_q}A'_{q,ac}$ should decrease while the amplitude $\left|K_{\Delta R_s,ac}\hat{i}_{d,dc}^e\right|$ remains unchanged. Furthermore, if there is no $L_q$ mismatch, $K_{\Delta L_q}A'_{q,ac}$ would be zero, and so would this part of the AC component. Therefore, for a given injected current signal, the accurate q-axis inductance can be determined when the amplitude of the AC component is minimised, and the correction of $L_q$ can be independently achieved without considering the effect due to $R_s$ deviations on position estimation. With accurate $L_q$, the related position error $\Delta\theta_{\Delta L_q}$ can be eliminated.

### B. AC SIGNAL SUPERIMPOSED ONTO D-AXIS TO MINIMISE EFFECT OF RESISTANCE MISMATCH

Similarly, to correct $R_s$, the sinusoidal current signal is superimposed onto $d$-axis current command $i_d^*$, and the corresponding $d$-axis current can be expressed as:

$$\hat{i}_d^e = \hat{i}_{d,dc}^e + \hat{i}_{d,ac}^e \quad (24)$$

Therefore, by substituting (24) into (18), it can be rewritten as:

$$\begin{aligned}\Delta\theta_{\Delta R_s,ac} &\approx K_{\Delta L_q}\hat{i}_{q,dc}^e + K_{\Delta L_q,ac}\hat{i}_{q,dc}^e + K_{\Delta R_s}\hat{i}_{d,dc}^e + K_{\Delta R_s}\hat{i}_{d,ac}^e \\ &= \Delta\theta_{par} + K_{\Delta R_s}\hat{i}_{d,ac}^e + K_{\Delta L_q,ac}\hat{i}_{q,dc}^e \end{aligned} \quad (25)$$

where

$$K_{\Delta L_q,ac} = \frac{\Delta L_q^2\hat{i}_{d,ac}^e}{\left(E_{ex}/\hat{\omega}_r^e + \Delta L_q\hat{i}_{d,dc}^e + \Delta L_q\hat{i}_{d,ac}^e\right)\left(E_{ex}/\hat{\omega}_r^e + \Delta L_q\hat{i}_{d,dc}^e\right)} \quad (26)$$

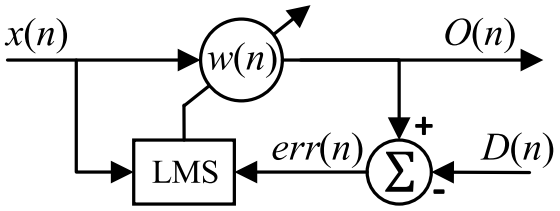


**FIGURE 5.** Block diagram of the LMS algorithm.

In (25), two extra terms $K_{\Delta R_s}\hat{i}^e_{d,ac}$ and $K_{\Delta L_q,ac}\hat{i}^e_{q,dc}$ appear due to d-axis current signal injection, and only the magnitude of $K_{\Delta R_s}\hat{i}^e_{d,ac}$ is related to the resistance mismatch. Therefore, by correcting the resistance parameter in the observer, the amplitude of the AC component in the position error can be minimised as well.

### C. AMPLITUDE CALCULATION TECHNIQUE

From the above analysis, the amplitude of the AC component in position error is the critical information to determine whether the parameters in the observer are mismatched or not. Therefore, the AC component has to be extracted and used for amplitude calculation. However, it is impossible to access the position error $\Delta\theta_{par}$ directly. Thus, it is more convenient to extract the AC component from the estimated speed signal $\hat{\omega}_r$ instead, since it is the derivative of the estimated position. With the help of a peaking filter, the AC component $\hat{\omega}_r^{ac}$ that is contained in $\hat{\omega}_r$ can be extracted. The transfer function of a peaking filter is expressed as [23]:

$$G(s) = \frac{\mu s}{s^2 + \mu s + \omega_{ac}^2} \tag{27}$$

where $\mu$ is the bandwidth of the peaking filter. Then, the amplitude $\left|\hat{\omega}_r^{ac}\right|$ of the AC component $\hat{\omega}_r^{ac}$ can be calculated through the orthogonal generation system which is based on a second-order generalised integrator (SOGI) [24].

### D. AMPLITUDE CALCULATION TECHNIQUE

As aforementioned, $\left|\hat{\omega}_r^{ac}\right|$ has a close relationship with the parameter mismatch. In order to find the accurate parameter, the minimum value of $\left|\hat{\omega}_r^{ac}\right|$ should be acquired by adjusting the parameter that is set in the observer. To accomplish this task, the LMS algorithm is used. The structure of the algorithm is shown in Fig. 5, which is a single-node network structure.

The algorithm operates in the discrete-time domain and $n$ denotes the n$^{\text{th}}$ sampling point. The output signal $O(n)$ can be expressed as: $O(n) = x(n)w(n)$, and the error $err(n)$ can be defined as the difference between the desired response $D(n)$ and the output signal $O(n)$, as: $err(n) = D(n)$-$O(n)$. The objective of this algorithm is to find a proper weight factor $w(n)$ to produce the least mean squares of $err(n)$. Thus, in this paper, the parameters ($\tilde{L}_q$ or $\tilde{R}_s$) of the sensorless observer are considered as the weight factors and $\left|\hat{\omega}_r^{ac}\right|$ is the input signal of the algorithm. Then, the error can be expressed as (take $\tilde{L}_q$ for example):

$$err\,(n) = D(n) - O\,(n) = 0 - \left|\hat{\omega}_r^{ac}\right|(n)\,L_q\,(n) \tag{28}$$

where the desired response $D(n)$ has set to zero. In (28), with a proper $L_q\,(n)$, $\left|\hat{\omega}_r^{ac}\right|(n)$ will be minimised when the error is minimised. Thus, when the objective function of the LMS algorithm $J\,(n)$ is defined as half of the squared error criterion: $J\,(n) = 0.5\,[err\,(n)]^2 = 0.5\left[-\left|\hat{\omega}_r^{ac}\right|(n)\,L_q\,(n)\right]^2$. The $L_q$ can be trained by applying a gradient descent method to minimise the objective function, as:

$$\begin{aligned} L_q\,(n+1) &= L_q\,(n) + \xi\,[-\nabla J\,(n)] \\ &= L_q\,(n) - \xi\left[\left|\hat{\omega}_r^{ac}\right|(n)\right]^2 L_q\,(n) \end{aligned} \tag{29}$$

where $\nabla J\,(n)$ is the gradient and $\xi$ is the training constant which determines the speed of convergence, the bigger the $\xi$, the faster the convergence. The weight factors are updated in the reverse direction of the gradient $\nabla J\,(n)$ since the value of the cost function needs to be reduced. Therefore, with the help of the LMS algorithm, $L_q\,(n)$ can be trained to accurate value adaptively and then the position error can be compensated. The procedure for resistance mismatch correction is basically the same, the only difference is that the sinusoidal current signal should be superimposed onto the $d$-axis current reference instead of the $q$-axis.

In (29), it is assumed that $L_q\,(n) > L_q\,(n+1)$, and the parameter is trained in the direction of decrease. However, the initial value of the parameter in the observer may be smaller or larger than the actual value before the correction, and the right direction of correction (decrease or increase) can be solved with the direction judgement strategy. In the paper, the technique used for initial direction judgment borrows the idea from Perturb and Observe algorithm, which is widely used in photovoltaic [30] and wind energy conversion system [31] for maximum power point tracking. It is based on the following criterion: if the adapting parameter is perturbed in a given direction and if $\left|\hat{\omega}_r^{ac}\right|$ decreases, it means that the parameter has moved towards the accurate value. Otherwise, if $\left|\hat{\omega}_r^{ac}\right|$ increases, the parameter has moved away from the accurate value, and therefore, the direction of the perturbation must be reversed. Take the very first cycle (n = 1) as an example, where the adjustment rule is defined as:

$$L_q(1) = L_q(0) - \Delta L_{step}(0), \quad \left(\Delta L_{step}(0) > 0\right) \tag{30}$$

where $L_q(0) = \tilde{L}_q$ represents the $q$-axis inductance value set in the observer initially, whilst $L_q(1)$ is the value after the first cycle training and $\Delta L_{step}(0) = \xi\left[\left|\hat{\omega}_r^{ac}\right|(0)\right]^2 L_q\,(0)$. After the first adjustment cycle, the training direction can be determined with the following logical judgement.

$$\begin{aligned} &if\ \left|\hat{\omega}_r^{ac}\right|_{L_q(0)} > \left|\hat{\omega}_r^{ac}\right|_{L_q(1)} \Rightarrow Correct\ Direction \\ &elseif\ \left|\hat{\omega}_r^{ac}\right|_{L_q(0)} < \left|\hat{\omega}_r^{ac}\right|_{L_q(1)} \Rightarrow Incorrect\ Direction \end{aligned} \tag{31}$$

where $\left|\hat{\omega}_r^{ac}\right|_{L_q(0)}$ and $\left|\hat{\omega}_r^{ac}\right|_{L_q(1)}$ represent the amplitudes of AC components when $L_q$ is set to $L_q(0)$ and $L_q(1)$ respectively.

The above procedure may be repeated once or twice to confirm that the correction is in the right direction. Moreover, various techniques can be applied to secure direction

judgment in practical application. For example, the step of adjustment can be set bigger than the defined to reduce the effect of noise and unexpected disturbance; Or by using the moving average value of $\left|\hat{\omega}_r^{ac}\right|$ to improve the accuracy of the direction judgment. With the help of these techniques, the correct direction of judgment can be guaranteed.

### E. EFFECTS OF CROSS-COUPLING AND INCRE-MENTAL INDUCTANCE

The cross-coupling effect is well known as the major source of position error in saliency-based methods [33], [34]. It could also introduce position errors in fundamental model-based methods, which can be easily compensated offline by using the technique in [4]. Although the test machine in this paper is an SPMSM with negligible cross-coupling effect, for the general feasibility of the proposed method, it is still worthwhile to investigate if the inaccuracy or neglect of $L_{dq}^{inc}$ could influence the accuracy of the $q$-axis inductance correction method. Moreover, the effect of incremental inductance due to current signal injection should also be investigated. Therefore, in this part, through the theoretical analysis, it would be shown that the effects of cross-coupling and incremental inductance have little impact on the accuracy of the proposed inductance correction method.

In the case of q-axis inductance mismatch, a sinusoidal current signal (20) with low frequency $\omega_{ac}$ and amplitude $A_{ac}$ is superimposed onto the q-axis current in the proposed correction method. However, at a steady-state, if the error between the estimated and actual current exists, and by considering the cross-coupling effect and incremental inductance, the d-axis E-EMF estimation error can be obtained for q-axis inductance deviation, as:

$$\begin{aligned}\varepsilon_{d,\Delta L_q} &= -\omega_r^e \Delta L_q \left(\hat{i}_{q,dc}^e + i_{ac}^*\right) - L_{dq}^{inc}\left(p\hat{i}_{ac}^* - pi_{ac}^*\right) \\ &= -\omega_r^e \Delta L_q \left(\hat{i}_{q,dc}^e + i_{ac}^*\right) - L_{dq}^{inc}\varepsilon_{ac,\Delta L_q} \end{aligned} \tag{32}$$

where $\varepsilon_{ac,\Delta L_q}$ is defined as the steady-state error of current derivative as $\varepsilon_{q,\Delta L_q} = p\hat{i}_{ac}^* - pi_{ac}^*$.

Similarly, the q-axis E-EMF estimation error can be acquired as:

$$\varepsilon_{q,\Delta L_q} = \omega_r^e \Delta L_q i_{d,dc}^e - L_d^{inc} g_q \varepsilon_{ac,\Delta L_q} \tag{33}$$

Therefore, the position error due to q-axis inductance mismatch can be calculated by substituting (32) and (33) into position error equation (15) as (34) when the effects of cross-coupling and incremental inductance are considered:

$$\begin{aligned}&\Delta\theta'_{\Delta L_q,ac} \\ &= \tan^{-1}\left(\frac{\varepsilon_{d,\Delta L_q}}{E_{ex} + \varepsilon_{q,\Delta L_q}}\right) \\ &= \tan^{-1}\left(\frac{-\Delta L_q\left(\hat{i}_{q,dc}^e + i_{ac}^*\right) - L_{dq}^{inc}\varepsilon_{ac,\Delta L_q}/\omega_r^e}{E_{ex}/\omega_r^e + \Delta L_q i_{d,dc}^e - L_d^{inc} g_q \varepsilon_{ac,\Delta L_q}/\omega_r^e}\right) \\ &\approx \frac{-\Delta L_q\left(\hat{i}_{q,dc}^e + i_{ac}^*\right) - L_{dq}^{inc}\varepsilon_{ac,\Delta L_q}/\omega_r^e}{E_{ex}/\omega_r^e + \Delta L_q i_{d,dc}^e - L_d^{inc} g_q \varepsilon_{ac,\Delta L_q}/\omega_r^e} \end{aligned} \tag{34}$$

where $g_q$ is the observer gain for the q-axis. From (34), the AC component of the position error that varies at the same frequency as the injected current signal can be expressed as:

$$\Delta\theta_{par,ac} = \frac{-\Delta L_q i_{ac}^* - L_{dq}^{inc}\varepsilon_{ac,\Delta L_q}/\omega_r^e}{E_{ex}/\omega_r^e + \Delta L_q i_{d,dc}^e - L_d^{inc} g_q \varepsilon_{ac,\Delta L_q}/\omega_r^e} \tag{35}$$

Therefore, if the effects of cross-coupling and incremental inductance to the proposed correction method are considered, the position error expression can be updated to (35) from the above analysis. As the goal of the correction procedure is to make sure that the numerator of position error equation (35) goes to the minimum value when q-axis inductance is adjusted, the extra term that is related to the d-axis incremental inductance $(-L_d^{inc} g_q \varepsilon_{ac,\Delta L_q}/\omega_r^e)$ in the denominator has no effects on the correction accuracy, and the two terms contained in the numerator should be paid more attention.

By close looking into the numerator in (35), it can be noticed that the term that is related to the incremental mutual inductance $-L_{dq}^{inc}\varepsilon_{ac,\Delta L_q}/\omega_r^e$ may have impact in searching for the minimum amplitude $\left|\hat{\omega}_r^{ac}\right|$. However, from the expression of this term, it can be analysed that it has little effect on the accuracy of q-axis inductance correction for several reasons: Firstly, the effect of this term reduces as the speed of the machine increases, thus, it can be neglected when the machine is running in a high-speed region. Secondly, the term could not affect the accuracy of q-axis inductance correction since the correction procedure aims to find the minimum amplitude value of the AC component in estimated speed, which may proportional to (36) from (35):

$$\sqrt{\left(\Delta L_q \left|i_{ac}^*\right|\right)^2 + \left(\left|L_{dq}^{inc}\varepsilon_{ac,\Delta L_q}\right|/\omega_r^e\right)^2} \tag{36}$$

From the second term of (36), its amplitude can be considered as a constant value during the injection procedure, and thus, when $\Delta L_q$ in first term of (36) is minimized, the whole amplitude can be minimized. Fig. 6 graphically represents the incremental and apparent inductances of the operation point for the proposed method, where the apparent inductance can be calculated from the slope of the flux linkage $\psi_o$ versus current through the operating point and the origin $i_o$, as $L^a = \psi_o/i_o$, and the incremental inductance can be calculated based on the perturbation method as $L^{inc} = \partial\psi_o/\partial i_o$. When the q-axis current is slightly oscillating around the operating point after the injection, $L^{inc}$ can be assumed to be constant. Therefore, with the small amplitude current signal injection (generally less than 5% of the rated current for the proposed method), $L_{dq}^{inc}$ can be considered as a constant value, and its effect on the amplitude would not change. Above all, the effect from the second part of (36) can always be minimised when the observer gain is well designed, and thus, the AC component of the estimated current $\hat{i}_{ac}^*$ is close to the applied $i_{ac}^*$ to make $\varepsilon_{ac,\Delta L_q}$ minimum. Since the magnitude of

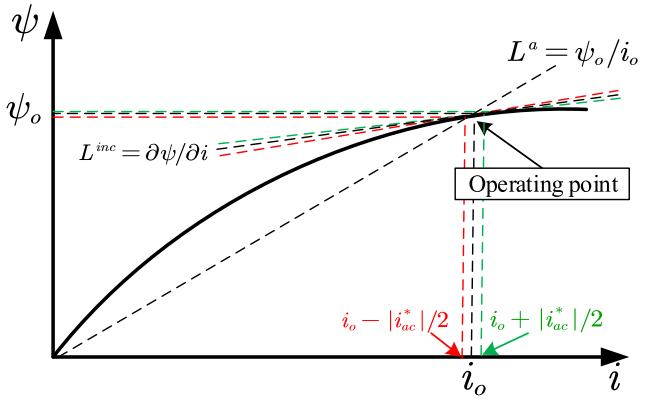


**FIGURE 6.** Effect of apparent inductance and incremental inductance representation for the proposed signal injection method.

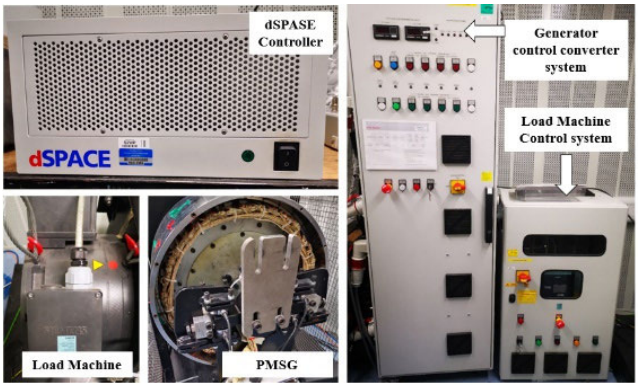


**FIGURE 7.** Experimental test rig.

$\varepsilon_{ac,\Delta L_q}$ is much smaller when compared to the amplitude of $i^*_{ac}$ in the first term of (36), which makes the second term that is related to the incremental inductance less important even more.

Therefore, the correction procedure can effectively find the minimum amplitude to accurately correct the q-axis inductance, and the accuracy of the proposed correction method cannot be influenced by the effects of cross coupling and incremental inductance.

Unlike the HF signal injection and INFORM sensorless methods, which are based on machine saliency, the proposed correction method incorporates with the fundamental model based sensorless method and injects low frequency and small amplitude sinusoidal current signals to obtain the corresponding response in estimated speed based on the position error mechanism. The proposed method is an online position error correction method. The corrected procedure of each parameter can be independently implemented when it is required, and the compensation can be accomplished in a very short period. In a real application, the technique can also be used during the commissioning of the drive system or can be employed as a one-shot test when the parameter tracking is required or becomes critical. In addition, the inductance value may change with load variation due to saturation effect. Therefore, to minimise the estimated position error, the parameters such as $q$-axis inductance in the observer need to be adapted accordingly for each operation point. Hence, the proposed correction method may need to be regularly applied during the machine operation, especially when the operation point is changed. However, once the inductance has been tuned for a given load point, there shall be no need for correction anymore unless other specific requirements are needed.

## V. EXPERIMENTAL VALIDATION

### A. EXPERIMENTAL SYSTEM

To validate the proposed technique, experiments are carried out on a downscaled representative wind turbine PM generator control system. The control is implemented based on a dSPACE DS1006 platform as shown in Fig. 7. The parameters of the tested SPMSM ($L_d \approx L_q$) are shown in Table 1. The switching frequency for the voltage source converter is set at 2500Hz, and the control sampling frequency takes the same rate. The actual rotor position can be acquired from a 12-bit incremental encoder, and the information is only used for comparison purposes but not for control. The speed of the generator is set and controlled by the load machine. The generator is controlled with a standard FOC torque control technique, and the rotor electrical position is estimated by the E-EMF method.

It should be also mentioned that apart from the deviation in parameters of inductance and resistance, the accuracy of position estimation could also be affected by the inverter nonlinearity, such as the dead time and the turn ON/OFF time, which would mainly introduce the 6$^{th}$ order harmonic position error [32]. In this paper, the method in [32] is used for inverter nonlinearity compensation. The spectra of measured position errors with/without inverter nonlinearity compensation are compared in Fig. 8 at 20 (1/min), 50% load condition when all the parameters are set to their actual values in the sensorless observer. It can be seen that by inverter nonlinearity compensation, the 6$^{th}$ order harmonic in position estimation is significantly reduced.

Since the position error due to possible resistance deviation and inverter nonlinearity is generally less significant than that from the inductance deviation at high speeds [8], the requirement on complete compensation of inverter nonlinearity may be relaxed. In addition, as the proposed method does not need to change the position observer, but only create an outer loop for the error correction, it can work together with any inverter nonlinearity compensation solutions that have been established.

The main reason for using torque control in experiments is because the estimated position error can be varied in relationship with the currents ($d$-axis for $\Delta R_s$ or $q$-axis for $\Delta L_q$ as investigated in Section III), and thus it is more convenient and direct to test the proposed estimated position correction method under the torque control conditions. Moreover, for practical application, such as offshore wind power control system, the speed control operation is normally performed with pitch and yaw control. The speed of the turbine generally has a low dynamic due to huge inertia. Thus, the

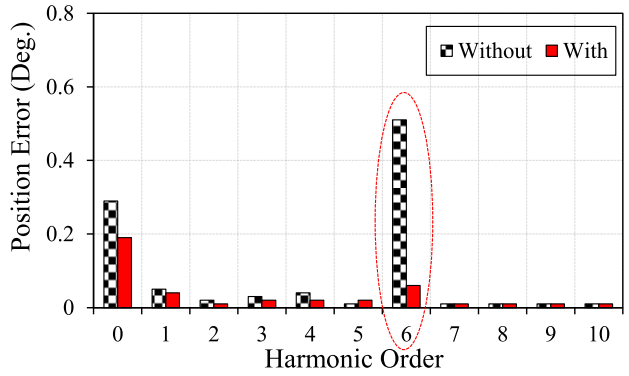


**FIGURE 8.** Comparison of results with/without inverter nonlinearity compensation.

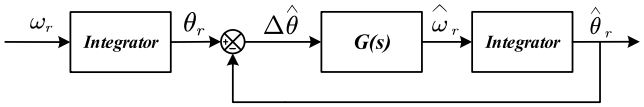


**FIGURE 9.** Equivalent block diagram of position and speed estimator.

proposed method can be applied during the steady-state conditions. For other applications where the speed control is from the machine side, the proposed method can still be applied directly to the current control loop when the steady-state condition is achieved, as long as the injected frequency is outside the speed control bandwidth.

### B. AMPLITUDE AND FREQUENCY SELECTION OF INJECTED SIGNAL

Since the feedback current is required to track the current reference variation properly with the same frequency as the signal injection, the frequency of the injected current signal $\omega_{ac}$ has to be lower than the current control loop bandwidth. Moreover, in order to avoid introducing unexpected oscillations, the frequency should be higher than the outer loop bandwidth, no matter it is for speed, torque, or power. Furthermore, it is recommended that the frequency selected should avoid 6 times of fundamental electrical frequency in case that the inverter nonlinearity is not well compensated.

In the extended EMF position observer, the position error $\Delta\hat{\theta}$ is derived from the estimated E-EMF in the estimated dq reference frame $\hat{e}^e_{dq}$, as (8), then the estimated speed and position are compensated by the regulator $G(s)$ to drive the position error $\Delta\hat{\theta}$ to zero. The procedure can be illustrated in a feedback system as shown in Fig. 9 [7].

In Fig. 9, G(s) is the proportional and integral (PI) regulator, which is applied to drive the estimated position to the expected one as the following transfer function:

$$\widehat{\theta}_r = \frac{K_p s + K_i}{s^2 + K_p s + K_i}\theta_r \tag{37}$$

where $K_p$ and $K_i$ are the proportional and integral gains, respectively, which determine the estimating performance. They can be expressed as (38) when the natural frequency $\omega_n$ and the damping ratio $\zeta_n$ in the feedback system (Fig. 9) are designed.

$$K_p = 2\zeta_n\omega_n, \quad K_i = \omega_n^2 \tag{38}$$

For a given position observer, where the speed and position estimator may have already been tuned for the application, i.e. a certain bandwidth has been defined, the frequency of the current signal injection should be set below the observer bandwidth. This is to maximise the response sensitivity to the current signal injection, and also to minimise the effect from incremental inductances.

If the sinusoidal current signal is superimposed onto $q$-axis current reference, the amplitude of the signal has to be small enough to not introduce torque ripples that may be unacceptable by the system. More factors may need to be considered depending on the different practical applications. In this paper, the amplitude and frequency are chosen as 0.2A and 25Hz respectively as an example for the test system. The test was performed on a representative direct-drive generator of wind turbine that has relatively high inertia. Therefore, with the selection of injection, the real speed hardly varies. On the other hand, for the low-inertia systems that may react to the q-axis current injection, the magnitude and frequency of the injected current signal can be selected so that its impacts on the system can be minimised. For example, the frequency could be chosen to avoid the mechanical resonance of the system, and the instant of injection can also be managed to prevent the possible interference between speed/torque harmonics and the correction procedure. Moreover, the magnitude can be set small, as only the relative change in response during parameter correction is used. The capability of fast correction, and thus the need of only a short time of injection, would also help.

In order to reduce the unexpected effects that may be introduced, the correction procedure should be applied when the system is in a relatively stable state of speed and load. For practical application, such as the PM generator of wind turbine applications for offshore, since the blades have a relatively large inertia and a low dynamic in speed, and the offshore wind condition is not frequently varied, the steady-state can be achieved and kept.

### C. EXPERIMENTAL PROCEDURE AND ANALYSIS OF RESULTS

The configuration of the sensorless control system with the parameter correction method has been shown in Fig. 10. The injection procedure controller is used to control which axis the signal is injected into based on the mismatch situation. The correction for $L_q$ and $R_s$ mismatch could be taken independently or in series.

Initially, with the help of an E-EMF sensorless observer, the estimated position and speed can be acquired. The parameters in the observer can be set to their nominal values or other values that may introduce larger parameter mismatch intentionally. When the correction procedure starts, the sinusoidal current signal is injected into the system ($q$- or $d$-axis of current), then AC component should appear in the estimated

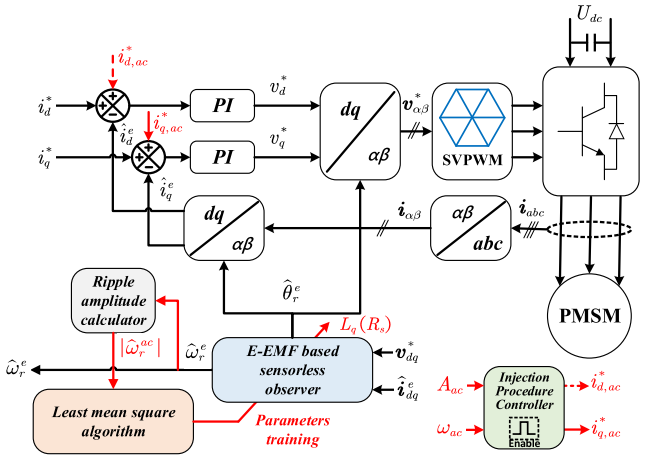


**FIGURE 10.** Block diagram of the proposed sensorless control system with the LMS parameter correction method.

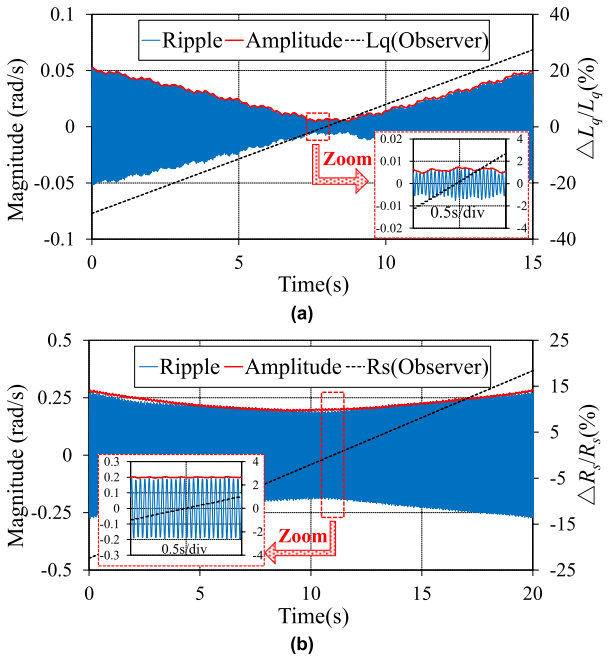


**FIGURE 11.** Extracted speed ripple $\hat{\omega}_r^{ac}$, amplitude $|\hat{\omega}_r^{ac}|$ according to parameter variation at 50% load condition. (a) $L_q$ variation when signal is injected into q-axis at 40(1/min). (b) $R_s$ variation when signal is injected into d-axis at 20(1/min).

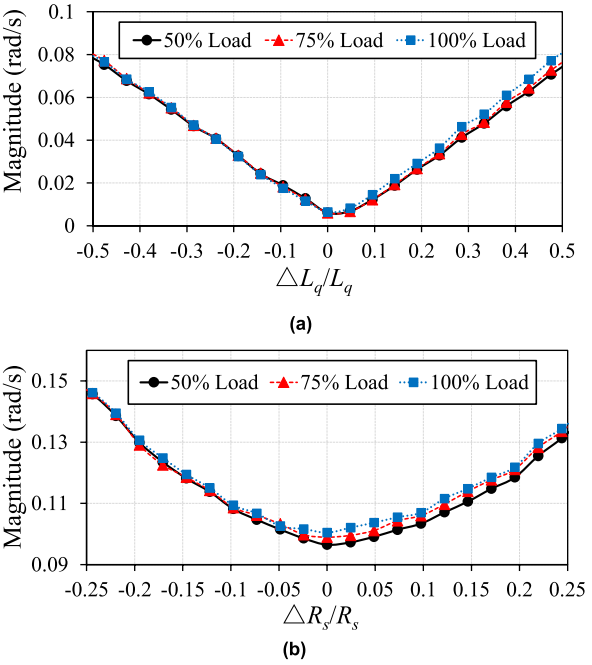


**FIGURE 12.** Measured $|\hat{\omega}_r^{ac}|$ versus mismatched ratio of different load conditions at 40(1/min). (a) $L_q$ mismatch when signal is injected into q-axis and Id = 0A. (b) $R_s$ mismatch when signal is injected into d-axis and Id = −2A.

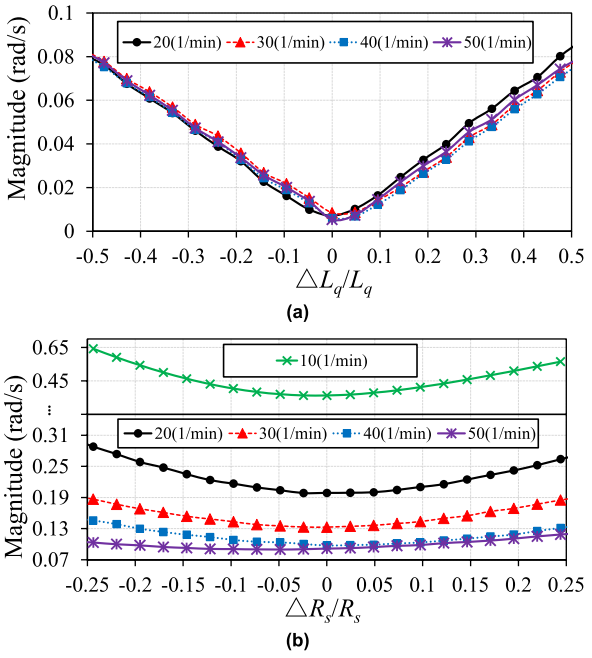


**FIGURE 13.** Measured $|\hat{\omega}_r^{ac}|$ versus mismatched ratio of different speed conditions at 50% load condition. (a) $L_q$ mismatch when signal is injected into q-axis and Id = 0A. (b) $R_s$ mismatch when signal is injected into d-axis and Id = −2A.

speed. The corresponding amplitude can be acquired from the amplitude calculator. At last, the LMS algorithm can train the parameter adaptively to a more accurate value compared with the original ones, and the injection can be stopped. With the updated parameters, the estimated position error caused by parameter mismatch should be corrected.

Fig.11 shows the extracted AC component $\hat{\omega}_r^{ac}$ and the amplitude $|\hat{\omega}_r^{ac}|$ variation for different parameter mismatch ratio ($\Delta L_q/L_q$, $\Delta R_s/R_s$) under the load condition of 50%, respectively. The sinusoidal current signal (0.2A, 25Hz) is superimposed onto the $q$-axis for $L_q$ mismatch or $d$-axis for $R_s$ mismatch. From Fig.11, it can be verified that the minimum point of $|\hat{\omega}_r^{ac}|$ corresponds to the non-mismatched $L_q$ or $R_s$ respectively ($\Delta L_q/L_q = 0$, $\Delta R_s/R_s = 0$), and $|\hat{\omega}_r^{ac}|$ decreases as the level of mismatch decreases.

Furthermore, in Fig.12, the influence of the load variation on $|\hat{\omega}_r^{ac}|$ has been evaluated for $L_q$ and $R_s$ mismatches at 40(1/min), respectively. Fig.12 shows that the load variation has very little effect on $|\hat{\omega}_r^{ac}|$ value. However, for change in

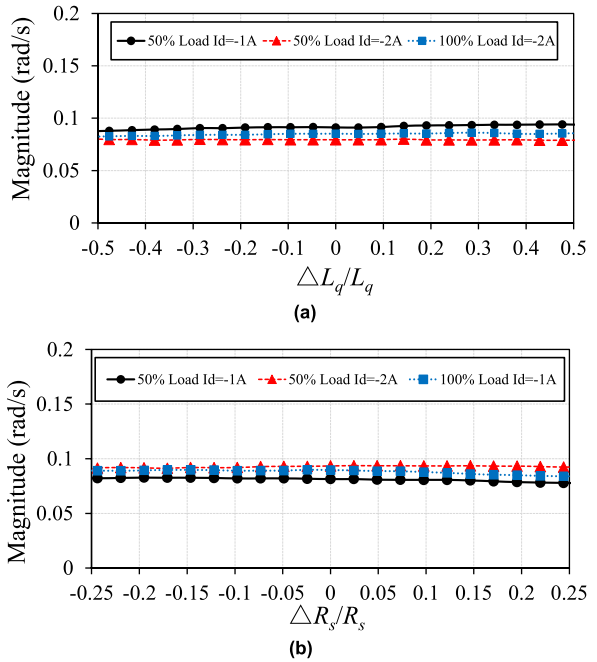


**FIGURE 14.** Measured $|\hat{\omega}_r^{qc}|$ versus mismatched ratio of different load conditions at 40(1/min). (a) $L_q$ mismatch when signal is injected into d-axis. (b) $R_S$ mismatch when signal is injected into q-axis.

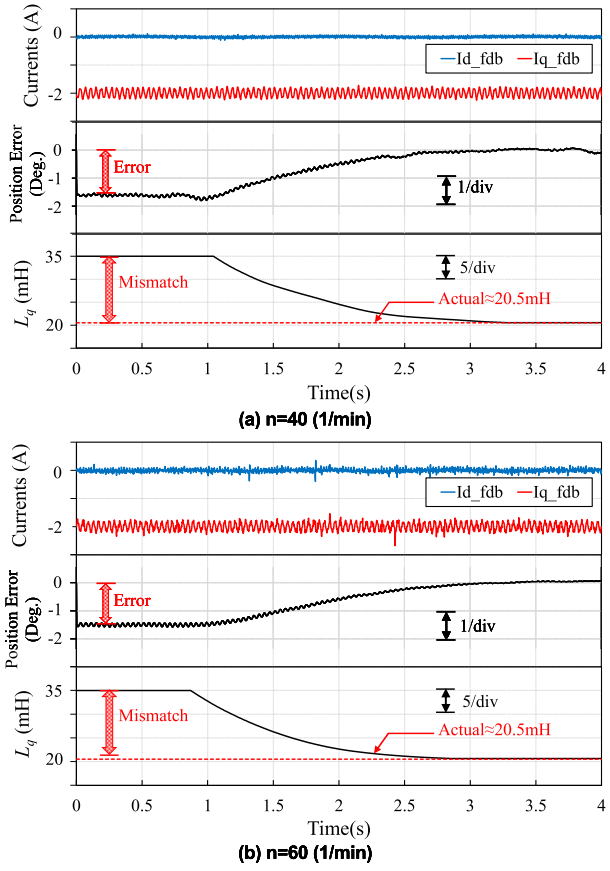


**FIGURE 15.** Measured position correction results of $L_q$ mismatch at 50% load condition when the signal is injected into q-axis current.

speed, as illustrated in Fig.13, since $K_{\Delta L_q}$ is independent of speed whereas $K_{\Delta R_s}$ is inversely proportional to the speed

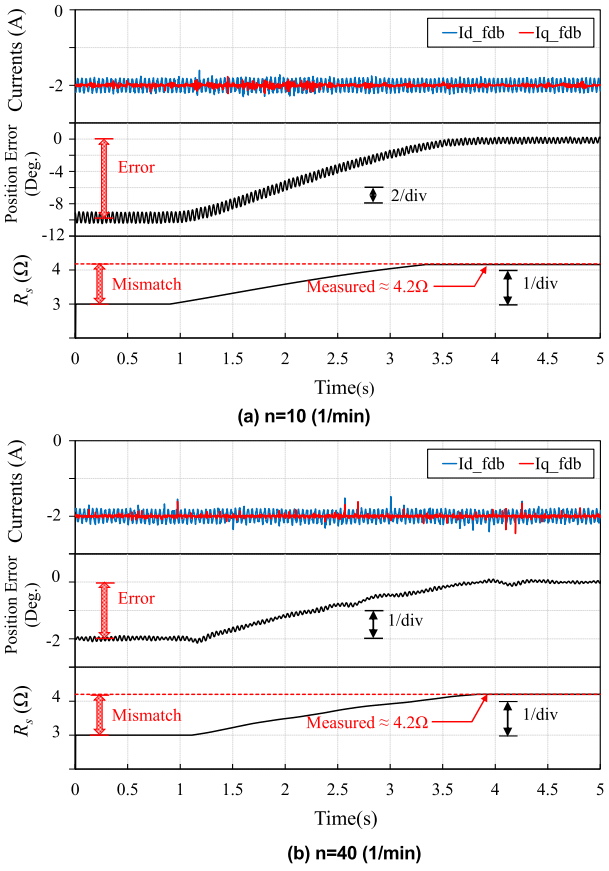


**FIGURE 16.** Measured position correction results of $R_S$ mismatch at 50% load condition when the signal is injected into d-axis current.

as (19), thus $|\hat{\omega}_r^{ac}|$ due to resistance mismatch reduces as the speed increases. Therefore, it is more effective to correct the resistance in low speed rather than high-speed region. In Fig.14(a), for the case of $L_q$ mismatch, instead of injecting the current signal into $q$-axis, it is injected into $d$-axis in order to see the influence of the variation. It can be seen that $L_q$ variation has little effect on $|\hat{\omega}_r^{ac}|$. Similarly, Fig.14(b) shows that the resistance variation has barely effect on $|\hat{\omega}_r^{ac}|$, when the current signal is injected into $q$-axis instead of d-axis. This confirms that the position errors caused by mismatched $L_q$ and $R_s$ can be decoupled and can be independently corrected.

By applying the LMS algorithm, the correction results can be shown in Figs. 15 and 16 for $L_q$ and $R_s$ mismatches, respectively, where the signals of feedback current, actual position error and corrected parameter are included. In Fig. 15(a), the machine is running at speed n = 40(1/min), while in Fig. 15(b) the speed is at n = 60 (1/min), and the initial nominal $L_q$ is set at 35mH in the observer and the current signal is injected into $q$-axis. After the LMS algorithm is enabled, $L_q$ is trained to approach the actual value, which is approximately 20.5mH, then the position error caused by $L_q$ mismatch can be removed. Similarly, for the case of $R_s$ mismatch, the test machine is rotating at 10(1/min) in Fig.16(a), while the speed is set to 40(1/min) for Fig.16(b). For both conditions, the nominal value is set to 3Ω initially, and by

applying the proposed technique, the mismatched $R_s$ can be corrected to the actual value of 4.2Ω, and the position error can be eliminated. From (16), when $\hat{i}_d^e = 0$, there should be no position error due to resistance mismatch. Therefore, the magnitude of the $d$-axis current in the test (Fig. 16) is only used for the validation purpose since the position error and the correction procedure can be clearly seen during the test when $\hat{i}_d^e \neq 0$. For SPMSM under $\hat{i}_d^e = 0$ control strategy, the extra sinusoidal current signal injection is only needed when $R_s$ correction is required, and since the correction can be accomplished in a very short period, it will not introduce much losses. It is noticed that with the same $R_s$ mismatch, the position error at low speed, Fig.16(a), is much greater than (b) when the speed is high. This is because that the position error due to $R_s$ mismatch decreases as the speed increases. Moreover, the corrected $R_s$ is normally higher than the machine phase resistance in design, since the observer operates with the average phase resistance of the system, which could include the effects of cable, inverter, and winding temperature variation.

## VI. CONCLUSION

In this paper, for the fundamental model based sensorless methods, the position error mechanism is derived, and then a simple but effective technique that is based on this error mechanism has been proposed to correct the position error. The error is caused by parameter mismatches in the sensorless observers, and it has been proven mathematically and experimentally that the error is mainly introduced by $R_s$ or $L_q$ mismatch and can be proportionally varied according to the d- or q-axis current (d-axis for $R_s$ mismatch or $q$-axis for $L_q$ mismatch). Therefore, when a suitable sinusoidal current signal is injected into the $d$- or $q$- current for a short period, the existence of a corresponding parameter mismatch can be revealed by detecting the AC component that appears in the estimated speed. With the help of the LMS algorithm, the amplitude of the AC component can reach the minimum value by training the parameter to its accurate value, and hence the position error in the sensorless observer can be corrected. The correction procedure for $L_q$ or $R_s$ mismatch can be independently applied without considering the effect of the accuracy of other parameters, and also will not suffer from the rank deficient and ill convergence issues. The proposed method has been validated through experiments for different operating conditions on a PM generator control system, and can be incorporated into other types of model-based sensorless methods.

## REFERENCES


[1] J.-H. Jang, S.-K. Sul, J.-I. Ha, K. Ide, and M. Sawamura, "Sensorless drive of surface-mounted permanent-magnet motor by high-frequency signal injection based on magnetic saliency," *IEEE Trans. Ind. Appl.*, vol. 39, no. 4, pp. 1031–1039, Jul. 2003.

[2] G. Foo and M. F. Rahman, "Sensorless sliding-mode MTPA control of an IPM synchronous motor drive using a sliding-mode observer and HF signal injection," *IEEE Trans. Ind. Electron.*, vol. 57, no. 4, pp. 1270–1278, Apr. 2010.

[3] S. Morimoto, M. Sanada, and Y. Takeda, "Mechanical sensorless drives of IPMSM with online parameter identification," *IEEE Trans. Ind. Appl.*, vol. 42, no. 5, pp. 1241–1248, Sep. 2006.

[4] Y. Li, Z. Q. Zhu, D. Howe, and C. M. Bingham, "Improved rotor position estimation in extended back-EMF based sensorless PM brushless AC drives with magnetic saliency," in *Proc. IEEE Int. Electr. Mach. Drives Conf.*, May 2007, pp. 214–219.

[5] S. Jurkovic and E. G. Strangas, "Design and analysis of a high-gain observer for the operation of SPM machines under saturation," *IEEE Trans. Energy Convers.*, vol. 26, no. 2, pp. 417–427, Jun. 2011.

[6] Z. Chen, M. Tomita, S. Doki, and S. Okuma, "An extended electromotive force model for sensorless control of interior permanent-magnet synchronous motors," *IEEE Trans. Ind. Electron.*, vol. 50, no. 2, pp. 288–295, Apr. 2003.

[7] S. Morimoto, K. Kawamoto, M. Sanada, and Y. Takeda, "Sensorless control strategy for salient-pole PMSM based on extended EMF in rotating reference frame," *IEEE Trans. Ind. Appl.*, vol. 38, no. 4, pp. 1054–1061, Jul. 2002.

[8] B. Nahid-Mobarakeh, F. Meibody-Tabar, and F. M. Sargos, "Back EMF estimation-based sensorless control of PMSM: Robustness with respect to measurement errors and inverter irregularities," *IEEE Trans. Ind. Appl.*, vol. 43, no. 2, pp. 485–494, Mar. 2007.

[9] S. Ichikawa, M. Tomita, S. Doki, and S. Okuma, "Sensorless control of synchronous reluctance motors based on extended electromotive force model and inductance measurement," *IEEJ Trans. Ind. Appl.*, vol. 125, no. 1, pp. 16–25, Jan. 2005.

[10] J. Yoo, Y. Lee, and S.-K. Sul, "Back-EMF based sensorless control of IPMSM with enhanced torque accuracy against parameter variation," in *Proc. IEEE Energy Convers. Congr. Expo. (ECCE)*, Sep. 2018, pp. 3463–3469.

[11] Y. Lee, Y.-C. Kwon, and S.-K. Sul, "Comparison of rotor position estimation performance in fundamental-model-based sensorless control of PMSM," in *Proc. IEEE Energy Convers. Congr. Expo. (ECCE)*, Sep. 2015, pp. 5624–5633.

[12] K. Lu, X. Lei, and F. Blaabjerg, "Artificial inductance concept to compensate nonlinear inductance effects in the back EMF-based sensorless control method for PMSM," *IEEE Trans. Energy Convers.*, vol. 28, no. 3, pp. 593–600, Sep. 2013.

[13] I. Boldea, M. C. Paicu, and G. D. Andreescu, "Active flux concept for motion-sensorless unified AC drives," *IEEE Trans. Power Electron.*, vol. 23, no. 5, pp. 2612–2618, Sep. 2008.

[14] A. Yoo and S.-K. Sul, "Design of flux observer robust to interior permanent-magnet synchronous motor flux variation," *IEEE Trans. Ind. Appl.*, vol. 45, no. 5, pp. 1670–1677, Sep./Oct. 2009.

[15] Z. Q. Zhu, Y. Li, D. Howe, C. M. Bingham, and D. Stone, "Influence of machine topology and cross-coupling magnetic saturation on rotor position estimation accuracy in extended back-EMF based sensorless PM brushless AC drives," in *Proc. IEEE Ind. Appl. Annu. Meeting*, Sep. 2007, pp. 2378–2385.

[16] M. Rashed, P. F. A. MacConnell, A. F. Stronach, and P. Acarnley, "Sensorless indirect-rotor-field-orientation speed control of a permanent-magnet synchronous motor with stator-resistance estimation," *IEEE Trans. Ind. Electron.*, vol. 54, no. 3, pp. 1664–1675, Jun. 2007.

[17] B. Nahid-Mobarakeh, F. Meibody-Tabar, and F. M. Sargos, "Mechanical sensorless control of PMSM with online estimation of stator resistance," *IEEE Trans. Ind. Appl.*, vol. 40, no. 2, pp. 457–471, Mar. 2004.

[18] A. Piippo, M. Hinkkanen, and J. Luomi, "Adaptation of motor parameters in sensorless PMSM drives," *IEEE Trans. Ind. Appl.*, vol. 45, no. 1, pp. 203–212, Jan. 2009.

[19] K.-W. Lee, D.-H. Jung, and I.-J. Ha, "An online identification method for both stator resistance and back-EMF coefficient of PMSMs without rotational transducers," *IEEE Trans. Ind. Electron.*, vol. 51, no. 2, pp. 507–510, Apr. 2004.

[20] S. Ichikawa, M. Tomita, S. Doki, and S. Okuma, "Sensorless control of permanent-magnet synchronous motors using online parameter identification based on system identification theory," *IEEE Trans. Ind. Electron.*, vol. 53, no. 2, pp. 363–372, Apr. 2006.

[21] K. Liu, Q. Zhang, J. Chen, Z. Q. Zhu, and J. Zhang, "Online multiparameter estimation of nonsalient-pole PM synchronous machines with temperature variation tracking," *IEEE Trans. Ind. Electron.*, vol. 58, no. 5, pp. 1776–1788, May 2011.

[22] A. Kilthau and J. M. Pacas, "Parameter-measurement and control of the synchronous reluctance machine including cross saturation," in *Proc. IEEE-IAS Annu. Meeting Conf. Rec.*, vol. 4, Oct. 2001, pp. 2302–2309.

[23] M. Karimi-Ghartemani, S. A. Khajehoddin, P. K. Jain, A. Bakhshai, and M. Mojiri, "Addressing DC component in PLL and notch filter algorithms," *IEEE Trans. Power Electron.*, vol. 27, no. 1, pp. 78–86, Jan. 2012.
[24] M. Ciobotaru, R. Teodorescu, and F. Blaabjerg, "A new single-phase PLL structure based on second order generalized integrator," in *Proc. 37th IEEE Power Electron. Spec. Conf.*, Jun. 2006, pp. 1–6.
[25] Y. C. Shi, K. Sun, L. P. Huang, and Y. D. Li, "Online identification of permanent magnet flux based on extended Kalman filter for IPMSM drive with position sensorless control," *IEEE Trans. Ind. Electron.*, vol. 59, no. 11, pp. 4169–4178, Sep. 2012.
[26] B. Widrow and M. A. Lehr, "30 years of adaptive neural networks: Perceptron, Madaline, and backpropagation," *Proc. IEEE*, vol. 78, no. 9, pp. 1415–1442, Sep. 1990.
[27] S. J. Underwood and I. Husain, "Online parameter estimation and adaptive control of permanent-magnet synchronous machines," *IEEE Trans. Ind. Electron.*, vol. 57, no. 7, pp. 2435–2443, Jul. 2010.
[28] M. S. Rafaq, F. Mwasilu, J. Kim, H. H. Choi, and J.-W. Jung, "Online parameter identification for model-based sensorless control of interior permanent magnet synchronous machine," *IEEE Trans. Power Electron.*, vol. 32, no. 6, pp. 4631–4643, Jun. 2017.
[29] D. Gaona, O. Wallscheid, and J. Bocker, "Sensitivity analysis of a permanent magnet temperature observer for PM synchronous machines using the Monte Carlo method," in *Proc. IEEE 12th Int. Conf. Power Electron. Drive Syst. (PEDS)*, Dec. 2017, pp. 599–606.
[30] N. Femia, G. Petrone, G. Spagnuolo, and M. Vitelli, "Optimization of perturb and observe maximum power point tracking method," *IEEE Trans. Power Electron.*, vol. 20, no. 4, pp. 963–973, Jul. 2005.
[31] S. M. R. Kazmi, H. Goto, H.-J. Guo, and O. Ichinokura, "A novel algorithm for fast and efficient speed-sensorless maximum power point tracking in wind energy conversion systems," *IEEE Trans. Ind. Electron.*, vol. 58, no. 1, pp. 29–36, Jan. 2011.
[32] G. Wang, H. Zhan, G. Zhang, X. Gui, and D. Xu, "Adaptive compensation method of position estimation harmonic error for EMF-based observer in sensorless IPMSM drives," *IEEE Trans. Power Electron.*, vol. 29, no. 6, pp. 3055–3064, Jun. 2014.
[33] Y. Li, Z. Q. Zhu, D. Howe, C. M. Bingham, and D. A. Stone, "Improved rotor-position estimation by signal injection in brushless AC motors, accounting for cross-coupling magnetic saturation," *IEEE Trans. Ind. Appl.*, vol. 45, no. 5, pp. 1843–1850, Jul. 2009.
[34] B. Shuang, Z. Q. Zhu, and X. Wu, "Improved cross-coupling effect compensation method for sensorless control of IPMSM with high frequency voltage injection," *IEEE Trans. Energy Convers.*, early access, Jun. 29, 2021, doi: 10.1109/TEC.2021.3093361.
[35] E. Robeischl and M. Schroedl, "Optimized INFORM measurement sequence for sensorless PM synchronous motor drives with respect to minimum current distortion," *IEEE Trans. Ind. Appl.*, vol. 40, no. 2, pp. 591–598, Mar. 2004.

**T. Y. LIU** received the B.Eng. degree in control engineering from Northeastern University, Shenyang, China, in 2009, and the M.Sc. degree in electrical engineering from the University of New South Wales, Sydney, Australia, in 2014, respectively. He is currently pursuing the Ph.D. degree with The University of Sheffield, Sheffield, U.K. From 2014 to 2017, he was a Research and Development Engineer at Midea Welling Motor Technology Company Ltd., Shanghai, China. His current research interest includes the sensorless control of permanent magnet synchronous machines.

**Z. Q. ZHU** (Fellow, IEEE) received the B.Eng. and M.Sc. degrees in electrical engineering from Zhejiang University, Hangzhou, China, in 1982 and 1984, respectively, and the Ph.D. degree in electrical engineering from The University of Sheffield, Sheffield, U.K., in 1991.

Since 1988, he has been with The University of Sheffield, where he has also been a Professor with the Department of Electronic and Electrical Engineering, since 2000. He is currently the Royal Academy of Engineering/Siemens Research Chair and the Head of the Electrical Machines and Drives Research Group, the Academic Director of Sheffield Siemens Wind Power Research Centre, and the Director of the CRRC Electric Drives Technology Research Centre and Midea Electric Machines and Control Systems Research Centre. His current major research interests include the design and control of permanent magnet machines and drives for applications ranging from electric vehicles through domestic appliance to renewable energy.

Dr. Zhu is a fellow of the Royal Academy of Engineering, U.K., and the Institute of Engineering and Technology (IET), U.K. He was a recipient of the 2019 IEEE Industry Applications Society Outstanding Achievement Award and the 2021 IEEE Nikola Tesla Award.

**B. SHUANG** received the B.Eng. and M.Sc. degrees in electrical engineering from Huazhong University of Science and Technology, Wuhan, China, in 2009 and 2012, respectively. He is currently pursuing the Ph.D. degree with The University of Sheffield, U.K. From 2012 to 2016, he was with Electromechanical Business Unit Midea Group Ltd., China, as a Research Engineer to develop ac drive. His research interests include sensorless control of permanent-magnet brushless machines and power electronics.

**Z. Y. WU** received the B.Eng. and M.Sc. degrees in electrical engineering from Northeastern University, Shenyang, China, in 1985 and 1988, respectively, and the Ph.D. degree from The University of Sheffield, U.K., in 1999. He is currently working with Siemens Gamesa Renewable Energy. His main research interest includes the control of permanent-magnet brushless machines and drives.

**DAVID A. STONE** received the B.Eng. degree in electronic engineering from The University of Sheffield, Sheffield, U.K., in 1984, and the Ph.D. degree from the University of Liverpool, Liverpool, U.K., in 1989. He joined the Electrical Machines and Drives Group, The University of Sheffield, where he is currently a Professor of electrical engineering. His research interests include battery management, energy storage and conversion, and energy utilization and power electronic applications, including dc–dc and motor drive systems.

**MARTIN P. FOSTER** received the B.Eng. degree in electronic and electrical engineering, the M.Sc. (Eng.) degree in control systems, and the Ph.D. degree in power electronics from The University of Sheffield, Sheffield, U.K., in 1998, 2000, and 2003, respectively. In 2003, he became an Academic Staff Member with The University of Sheffield specializing in power electronic systems and became a Senior Lecturer, in 2010, a Reader, in 2014, and a Professor of energy storage and conversion, in 2017. His current research interests include the modeling and control of switching power converters, resonant power supplies, multilevel converters, energy storage management systems, piezoelectric transformers and power electronic packaging, and thermal management.